

# C-S-H/polyaniline nanocomposites prepared by in situ polymerization

Rouhollah Alizadeh · James J. Beaudoin ·  
Laila Raki · Victor Terskikh

Received: 21 June 2010/Accepted: 10 September 2010/Published online: 25 September 2010  
© Springer Science+Business Media, LLC 2010

**Abstract** Synthesis and characterization of a new cement-based polymer nanocomposite is reported. Calcium silicate hydrate (C-S-H) was prepared in the presence of aniline monomer followed by in situ polymerization to increase the degree of interaction between inorganic and organic phases. Two stoichiometrically different C-S-H systems were used. The properties of the C-S-H/polyaniline materials were studied using several analytical techniques including SEM, XRD, TGA,  $^{29}\text{Si}$  MAS NMR and FTIR. It is suggested that the in situ polymerization method can effectively be employed for producing a C-S-H/Polymer nanocomposite. The extent of molecular interaction with the polymer depends on the chemical composition of the C-S-H. Production of a new range of polymer-modified cement-based systems having improved environmental stability and mechanical performance is promising.

## Introduction

Application of nanotechnology in cement and concrete science has shown early promise for improving the properties and performance of concrete materials [1]. The preparation of inorganic/organic nanocomposites is a possible approach to achieve this goal. The advancements are

primarily obtained through the polymer-modification of the calcium silicate hydrate (C-S-H) phase. In the cement chemistry nomenclature C = CaO, S = SiO<sub>2</sub> and H = H<sub>2</sub>O. Enhanced engineering properties and improvement in the durability characteristics are key objectives in the preparation of cement-based nanocomposites. Several mechanisms have been suggested for the interaction of various organic molecules with the inorganic C-S-H systems. These include surface adsorption/grafting at the defect sites in the C-S-H silicate chain [2–4]; intercalation into the interlayer galleries of the C-S-H [5–9]; and covalent bonding of silylated co-polymers on the C-S-H surface [10–12]. The observed differences in the nature and extent of the C-S-H/polymer interactions in the previous studies are most likely due to the preparation method and type of the polymer.

The main ideas for the synthesis of polymer-layered silicate nanocomposites have been originally developed in clay science [13]. Clay minerals such as montmorillonite, unlike C-S-H, have a very high swelling capacity [14]. This is favorable for the polymer molecules to intercalate into the gallery regions. Thus, the methods applied in clay science that result in the formation of polymer intercalated nanocomposites have to be used cautiously in cement science. In general, in the studies of organically modified C-S-H systems, a small amount of the polymer is added either to pre-formed C-S-H or during the C-S-H synthesis. Polymer molecules are relatively large in size, which makes them very difficult to fully interact with the inorganic C-S-H materials that can accommodate only about a monolayer of water between their sheets [15]. In this study, the in situ polymerization technique is employed. This allows for the initial interaction of monomers with the C-S-H and makes the subsequent polymerization more effective. Polyaniline (PAn) was chosen as the organic

R. Alizadeh (✉) · J. J. Beaudoin · L. Raki  
Institute for Research in Construction, National Research  
Council Canada, 1200 Montreal Rd, Ottawa, ON K1A0R6,  
Canada  
e-mail: aali.alizadeh@nrc-cnrc.gc.ca

V. Terskikh  
Steacie Institute for Molecular Sciences, National Research  
Council Canada, 1200 Montreal Rd, Ottawa, ON K1A0R6,  
Canada

moiety. Its monomer, aniline, is a relatively small molecule and can be readily polymerized by introducing an oxidant to the system [16]. The size of the monomer molecule is important considering the interlayer distance in the C–S–H systems (which varies from about 0.9 to 1.4 nm depending on the C/S ratio) to increase the possibility of physical interactions involving the intercalation process. Polyaniline is an important conductive polymer that has excellent environmental stability [17]. It has been used successfully in the preparation of intercalated clay-based nanocomposites [16–19]. In this study, C–S–H was investigated for its capability to host the aniline and polyaniline guest molecules. Several analytical tools were employed to elucidate various aspects of the interaction of C–S–H with the aniline and polyaniline.

## Method

### Materials

C–S–H was prepared by mixing the stoichiometric amounts of calcium oxide and silica in excess water. Two compositionally different C–S–H materials were studied having C/S molar ratios of 0.8 and 1.2. These representative stoichiometries were selected based on the chemical and physical differences observed for two categories of C–S–H obtained above and below a C/S ratio of about 1.1 [20–22]. The CaO was freshly calcined from the reagent grade calcium carbonate (Sigma-Aldrich) at 900 °C. Reactive silica (CAB-O-SIL®, grade M-5 from Cabot Corporation) was heated at 110 °C to remove any surface adsorbed water. Distilled out-gassed water was added to the solid mixture of CaO and SiO<sub>2</sub> in the HDPE bottles (water/solid mass ratio ≈ 10) to initiate the pozzolanic reaction. C–S–H/aniline samples were prepared in a method similar to that used for the phase pure C–S–H except that the water contained aniline monomer. 2 mL of reagent grade aniline (C<sub>6</sub>H<sub>7</sub>N from Sigma-Aldrich, 99.5% purity) was dissolved using a magnetic stirrer in the 75 mL water in a beaker. Aniline has an oily appearance in water. Thus, it needs to be carefully mixed to obtain a well-dispersed aqueous solution. This solution (pH = 8.8) was added to the dry mix of the CaO and SiO<sub>2</sub> (C/S ratios = 0.8 and 1.2). It is noted that, in clay science, the addition of aniline to the layered silicate is generally conducted under low pH conditions obtained by adding HCl [16, 19]. This is not favorable in cement-based materials as it may result in the decalcification of the C–S–H. All the bottles were mounted on a rotating rack (speed = 16 rpm), and the reactions were continued for another 50 days. The gel-like materials were then filtered and washed several times with water. The phase pure C–S–H and C–S–H/aniline preparations were dried under vacuum for 4 days at room temperature.

In order to polymerize the aniline monomers, ammonium persulfate ((NH<sub>4</sub>)<sub>2</sub>S<sub>2</sub>O<sub>8</sub> from Sigma-Aldrich, 98% purity) was used as an external oxidant. Each dried C–S–H/aniline preparation (0.5 g) was first mixed in 100 ml of water using a magnetic stirrer (at about 300 rpm using level 4 in a Fisher Thermix Stirrer Model 120 MR). While stirring the suspension solution, 0.228 g of ammonium persulfate was added. The stirring was continued for 24 h at room temperature. The final material was filtered, washed several times, and dried under vacuum at room temperature for 4 days. The filtered C–S–H/polyaniline (C/S = 1.2) had a light orange-pinkish color whereas the other nanocomposite sample (C/S = 0.8) was nearly white. A similar color difference was observed between the original C–S–H/aniline samples. The difference in the color of the produced materials is suggested to be an indication of the different extent of interaction of C–S–H systems (depending on their stoichiometry) with the organic molecules. Pure polyaniline was separately produced by adding ammonium persulfate to the aqueous solution of the aniline. After drying, all the materials were stored in nitrogen-purged glass vials until used in various experiments.

### Characterization

The morphological changes due to the interaction of C–S–H precursor with polyaniline were investigated using a scanning electron microscope. Micrographs were acquired from the uncoated specimens using a Hitachi S-4800 instrument. An accelerating voltage of 1.2 kV and an emission current of 7 μA were applied at a working distance of about 3 mm to obtain images having greater resolution and more details of the surface features than those obtained with higher accelerating voltage and working distance as demonstrated previously [23]. The SEM pictures reported in this study were all acquired at 40 K magnification.

The changes in the  $d_{002}$  basal spacing of the samples were monitored using an X-ray diffraction technique. The XRD spectra were obtained using a Scintag XDS 2000 diffractometer using CuK<sub>α</sub> radiation (wavelength = 0.15405 nm) and a graphite monochromator. A diffraction angle range of  $2\theta = 5\text{--}15^\circ$  was used at a step size of 0.03° and a 7-s count interval with an accelerating voltage of 45 kV and current of 35 mA. The noise level in the spectra was reduced by replacing the curves with a moving average of five data points.

Simultaneous thermogravimetric and differential thermal analyses (TGA-DTA) were performed using a TA Instruments SDT Q-600. About 10 mg of the sample was heated from ambient to 1,000 °C at a rate of 10 °C/min under the flow of nitrogen gas (10 mL/min). The derivative mass loss and heat flow was analyzed using Universal Analysis 2000 software.

The  $^{29}\text{Si}$  MAS NMR spectra were recorded using a Bruker Avance 200 instrument operating at a  $^{29}\text{Si}$  resonance frequency of 39.73 MHz. A magic angle spinning (MAS) rate of 4 kHz was employed using a 7 mm MAS  $^1\text{H}/\text{X}$  Bruker probe. High-power proton decoupling (50 kHz) was employed during spectra acquisition. The relaxation delay between 4  $\mu\text{s}$  ( $\pi/4$ ) r.f. pulses was 60 s which was found sufficient for obtaining quantitative spectra. A total number of 1,420 scans were acquired for each spectrum. The  $^{29}\text{Si}$  NMR chemical shifts were referenced to external TMS at 0.0 ppm.

The Fourier transform infrared (FTIR) spectra were recorded on a Thermo Nicolet spectrometer (Model Nexus 870) equipped with an MTEC photoacoustic cell (Model 300). The test was conducted on the powder materials placed in a 10-mm diameter stainless steel pan. 100 scans were collected for each sample. The background was corrected using the carbon black standard reference sample. Helium was used as the purge gas (flow rate = 5 mL/s). Results were analyzed using OMNIC software (Nicolet Instruments).

## Results and discussion

### Scanning electron microscopy (SEM)

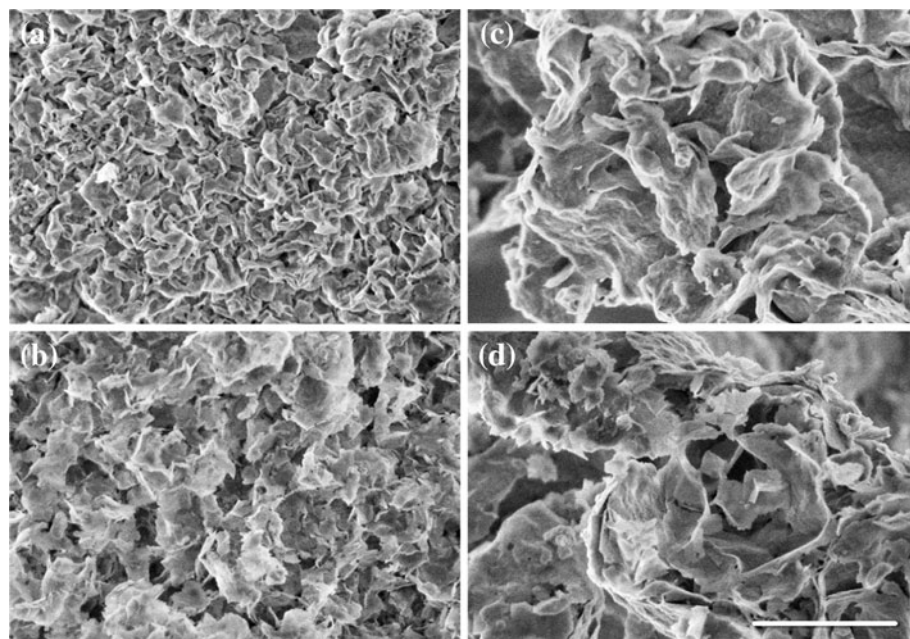
The micrographs acquired from the surface of the polymer modified C–S–H samples are compared in Fig. 1 with those obtained from the control samples. It is observed that the C–S–H has a platy or foil-like morphology. The size of the C–S–H plates appears to be dependent on the C/S ratio. Low lime C–S–H (Fig. 1a) is composed of smaller but densely connected plates compared to C–S–H having

C/S = 1.2 (Fig. 1c). The relatively high surface area of the C–S–H (C/S = 0.8) can easily be noticed. This is consistent with the nitrogen BET surface area measurements for this sample, 186  $\text{m}^2/\text{g}$ . The high lime C–S–H (C/S = 1.2) appears to have thicker and larger plates, and thus has lower BET surface area, 30  $\text{m}^2/\text{g}$ .

The morphology of the C–S–H is altered following the interaction with the polyaniline (Fig. 1b, d) although the main structural features are maintained. It appears that the C–S–H (C/S = 0.8) nanocomposite has thinner plates and a less dense structure. The SEM is not conclusive with regard to any significant change in the morphology of the polymer modified C–S–H (C/S = 1.2). This might be explained by assuming that the polyaniline molecules are interacted at the defect sites. The number of defect locations (i.e., missing bridging tetrahedra) is relatively larger at higher C/S ratio C–S–H [5]. The grafting of polyaniline molecules on the surface at these defect sites, may not change the morphology of the C–S–H (C/S = 1.2) as much as that in the 0.8 C/S ratio C–S–H.

Particles having morphology similar to that of the pure polyaniline (shown in Fig. 2) were not detected in either of C–S–H/polyaniline preparations. This may suggest that the polymer is intimately interacting with the nanostructure of the C–S–H and is not freely present in the nanocomposite samples as a separate phase. Moreover, the elemental analysis using energy dispersive X-ray technique (EDX) did not provide any evidence for the existence of regions containing only carbon atoms (the primary detectable atom in the polyaniline). The Si and Ca atoms were present in all the examined particles indicative of the absence of separately formed pure polyaniline (that would contain only detectable C atom) in the nanocomposite.

**Fig. 1** The representative SEM images of (a) C–S–H (C/S = 0.8), (b) C–S–H/polyaniline (C/S = 0.8), (c) C–S–H (C/S = 1.2), (d) C–S–H/polyaniline (C/S = 1.2) captured at 40 K magnification. The white scale bar indicates 1  $\mu\text{m}$



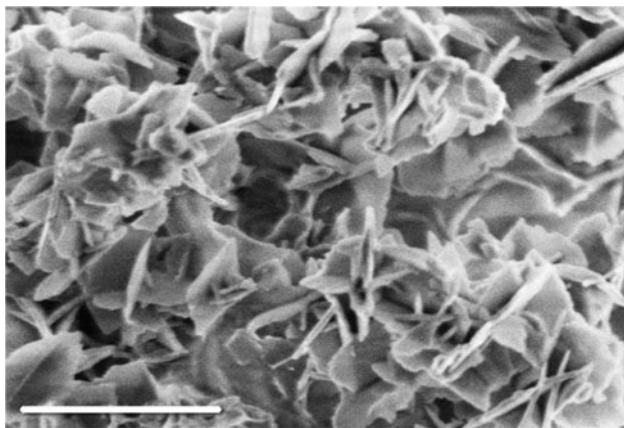


**Fig. 2** The SEM micrograph of the pure polyaniline prepared by the polymerization of aniline monomer using ammonium persulfate as an oxidant at room temperature. The white scale bar indicates 1  $\mu$ m

#### X-ray diffraction (XRD)

The main purpose of the XRD analysis was to investigate the change in the distance between the layers of C–S–H caused by possible interaction with aniline and polyaniline. The XRD spectra of the samples are shown in Fig. 3. Specifically, the region from  $2\theta = 5$ –12 degrees, where  $d_{002}$  basal spacing reflection occurs, is selected. The XRD peaks shown are somewhat broad indicative of the semi-crystalline nature of the synthetic C–S–H. There is a clear distinction between the basal spacing of the two phase pure C–S–H samples (Fig. 3a, d). The mean distance between the C–S–H sheets decreases as C/S ratio increases from about 1.17 nm (C/S = 0.8) to 0.97 nm (C/S = 1.2). This difference is possibly due to the existence of a larger number of bridging tetrahedra and Si–OH groups in the silicate chain of low C/S ratio C–S–H. The interlayer water occupies a similar space with thickness of about one water molecule in both C–S–H systems, and the total decrease in the basal spacing upon the removal of interlayer water from various C–S–H systems is essentially similar [15].

The semi-crystalline structure of the C–S–H formed in the aniline solution is preserved as supported by the existence of low angle basal spacing reflection (Fig. 3b, e). The basal spacing does not seem to be affected when the C–S–H is formed in the presence of aniline monomers compared to the control samples. It is, however, noticed that this peak broadens. It may be suggested that the monomer molecules, considering their relatively small size of about 0.2 nm [16], are most likely intercalated partially into the interlayer regions of C–S–H. This may result in an uneven change in the  $d_{002}$  basal spacing that is manifested by X-ray diffraction over a wider range of  $2\theta$ ; i.e., broader peaks. The XRD spectra of the samples after the polymerization of aniline are shown in Fig. 3c, f. It is unexpectedly observed that the basal spacing of the C–S–H is

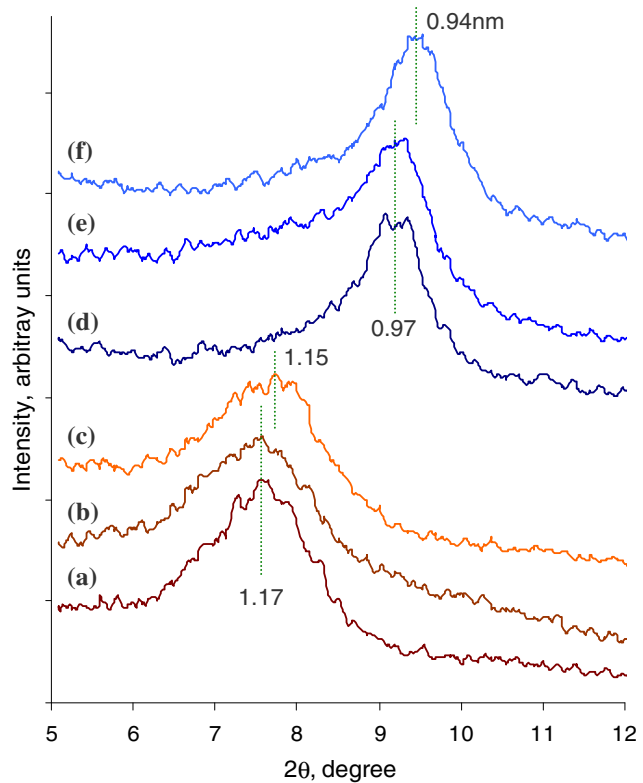


**Fig. 3** The XRD spectra showing the  $d_{002}$  basal reflection of (a) C–S–H (C/S = 0.8), (b) C–S–H/aniline (C/S = 0.8), (c) C–S–H/polyaniline (C/S = 0.8), (d) C–S–H (C/S = 1.2), (e) C–S–H/aniline (C/S = 1.2), (f) C–S–H/polyaniline (C/S = 1.2)

slightly decreased to about 1.15 nm and 0.94 nm for C/S = 0.8 and 1.2, respectively. The breadth of the peaks is similar to that in the C–S–H/aniline preparations. Other researchers have only reported either an increase [5–7] or no change [24, 25] in the distance between the layers of C–S–H when organically modified. It may be suggested that the aniline monomers situated initially at the end of interlayer galleries are removed to form the polyaniline during the polymerization process. This would slightly decrease the basal spacing. Another possible explanation is that the orientation and alignment of the rings in the polymer are different from those in the monomer molecules. The polyaniline may be positioned between the C–S–H layers in a way that the benzene ring is oriented parallel to the sheets. The monomer molecules, however, are most likely arranged randomly in various directions which results in higher basal spacing compared to that in the case of C–S–H/polyaniline samples after polymerization.

#### Thermogravimetric analysis (TGA)

The derivatives of the mass loss curves for C–S–H/polyaniline samples obtained through TGA are shown in Fig. 4 in comparison to those from the phase pure C–S–H and

C–S–H/aniline systems. The first peak, located between ambient temperature and about 250 °C, is associated with the removal of free, adsorbed, and interlayer water. It is also possible that the aniline monomers contribute to the mass loss in this region. In the both C–S–H/polyaniline samples, this peak is followed by a broader low intensity peak (240–460 °C) that is possibly due to the removal of constitutional water from the C–S–H crystal structure as reported earlier [26]. This peak was similar in the C–S–H and C–S–H/aniline preparations. After these events, there is no significant mass loss in all samples up to about 800 °C except for the C–S–H/polyaniline materials (Fig. 4). The derivative mass loss for the C/S = 1.2 C–S–H nanocomposite has a peak between 580 and 640 °C. This mass loss, that is about 0.94% of the solid mass, is attributed to the thermal decomposition of the polyaniline in the sample [27, 28]. This event is accompanied by an endothermal peak in the heat flow curves from differential thermal analysis (not shown). It is noticed that there is not a major mass loss in this region for the C–S–H and C–S–H/aniline preparations. The TGA result for the low lime sample (C/S = 0.8) contains a similar peak in the range of 580–640 °C. However, there is an additional smaller peak between 450 and 580 °C. It is suggested that this extra peak is also associated with the polyaniline decomposition.

It is likely that the polyaniline in this sample is formed in two different structural locations of C–S–H e.g., grafted on the surface and partially intercalated in the interlayer regions. The bond energy between the polymer and the inorganic base is possibly different in these locations. The mass loss at lower temperatures is likely associated with

the polyaniline that is physically adsorbed on the surface of C–S–H and therefore requires less energy for its decomposition. Higher temperature mass loss, on the other hand, can be attributed to the presence of stronger bonds between polyaniline and C–S–H (such as those related to the defect sites and interlayer regions). It is also possible that the polymer chain length and therefore its molecular mass would depend on the local environment in which the aniline monomer was polymerized [29, 30]. Therefore, the energy required to decompose the polyaniline is different for two distinct polyaniline materials manifested by a shift to lower temperatures. The total mass loss in the solid phase is about 1.58% for the low lime nanocomposite preparation (C/S = 0.8). The polymer content for this sample is almost 50% more than that for the high lime C–S–H/polyaniline sample. This is most likely due to the higher surface area of the C–S–H (C/S = 0.8) that provides more sites for the interaction with the polymer. Moreover, a larger content of monomer may have been initially interacted with the C/S = 0.8 C–S–H in comparison to the C/S = 1.2 C–S–H. The remainder of monomers not interacted with the C–S–H have been possibly removed during the washing process, and thus a lower amount of monomer was available for polymerization in the case of C/S = 1.2 C–S–H. The nitrogen BET surface area of the C–S–H is about 186 and 30 m<sup>2</sup>/g for C/S = 0.8 and 1.2, respectively. An estimate shows that the polyaniline loading was about 20% of the surface monolayer coverage in C/S = 0.8 C–S–H/polyaniline preparation, or about 40% of the available intercalation volume. In the C/S = 1.2 C–S–H/polyaniline preparation, the estimated polyaniline loading was even higher, at about 60% of the monolayer coverage, or 120% of the estimated intercalation capacity.

There is a final mass loss in all samples at about 810 °C, which is likely associated with the transformation of C–S–H to  $\beta$ -wollastonite [31].

#### <sup>29</sup>Si MAS NMR spectroscopy

The <sup>29</sup>Si NMR is a powerful technique for probing the nanostructure of the layered silicate hydrates including C–S–H [32]. It has also been employed to provide evidence for the interaction of organic substances with C–S–H [33]. The <sup>29</sup>Si MAS NMR spectra obtained for various C–S–H systems are shown in Fig. 5. The spectra of high C/S ratio C–S–H preparations (C/S = 1.2) contain two peaks at about –79.3 and –84.9 ppm. These peaks correspond to  $Q^1$  (end chain silicate tetrahedra) and  $Q^2$  (middle chain and bridging silicate tetrahedra), respectively [32]. It is observed that the relative intensity of  $Q^2$  to  $Q^1$ , which serves as an indication of the silicate polymerization, changes when the C–S–H is organically modified. In order

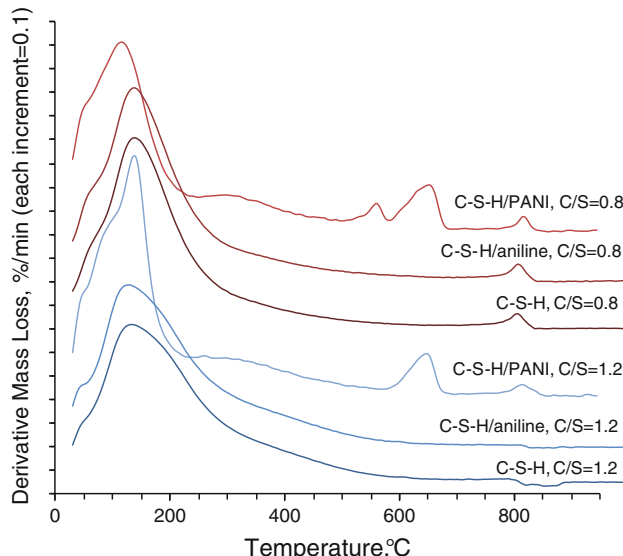


**Fig. 4** The derivative of the mass loss curves in TGA experiment for C–S–H, C–S–H/aniline, and C–S–H/polyaniline systems prepared at C/S ratios of 0.8 and 1.2. The curves are offset along y-axis for clarity

to examine the extent of silicate polymerization in these materials quantitatively, the spectra were deconvoluted using DMfit software [34]. The integral intensity of the simulated  $Q^1$  and  $Q^2$  peaks using Lorentzian line-shapes (not shown) are presented in Table 1. It is noted that the  $Q^2/Q^1$  ratio increases from 0.21 for the pristine phase pure sample to 0.63 in the polymer-modified C–S–H ( $C/S = 1.2$ ). The increase in the silicate polymerization of modified C–S–H system is attributed to the shielding effect of organic materials adsorbed at defect locations on the surface of the C–S–H as suggested previously for several other organically modified C–S–H nanocomposites [33]. Partial decalcification of the C–S–H during the polymerization (caused by the immersion in excess water and relatively low pH of the solution) as examined using EDX may partially be responsible for the increase in the silicate polymerization of the C–S–H [35]. It is noted, however, that a similar increase in the degree of silicate

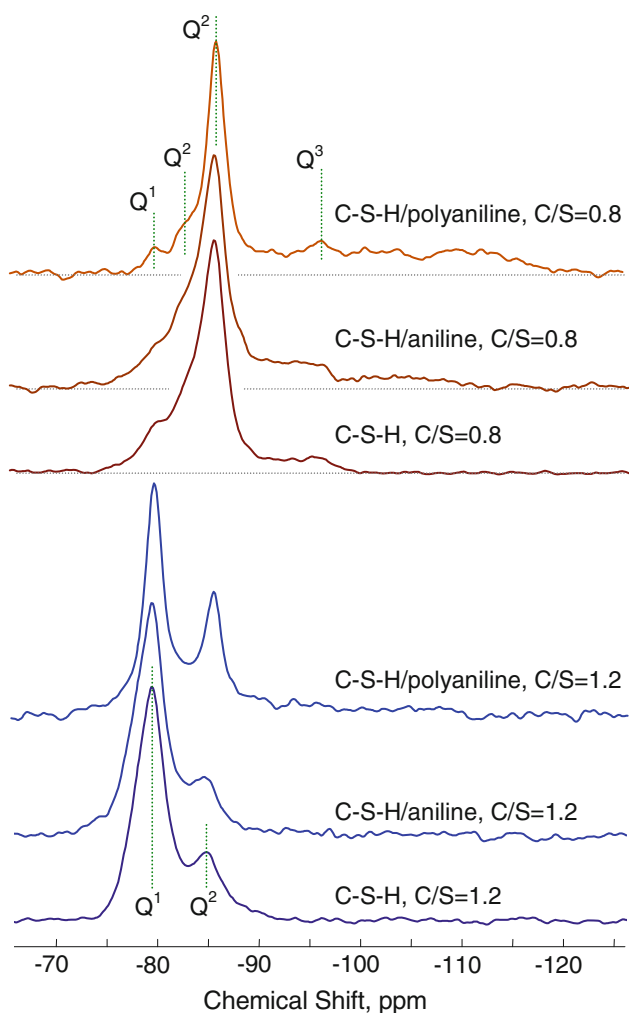


**Fig. 5** The  $^{29}\text{Si}$  MAS NMR spectra of the phase pure and organically modified C–S–H systems

**Table 1** Integral intensity (%) of the deconvoluted peaks in the  $^{29}\text{Si}$  MAS NMR spectra using Lorentzian lines

Sample	$Q^1$	$Q^2$	$Q^3$	$Q^4$	$Q^2/Q^1$
C/S = 1.2					
C–S–H	82.6	17.4	–	–	0.21
C–S–H/aniline	87.4	12.6	–	–	0.14
C–S–H/polyaniline	61.3	38.7	–	–	0.63
C/S = 0.8					
C–S–H	8.6	86.6	4.8	–	10.1
C–S–H/aniline	3.1	75.9	11.4	9.6	24.7
C–S–H/polyaniline	1.7	48.9	28.8	20.6	28.1

polymerization of C–S–H–polymer nanostructures has been previously reported even when the reagents are not interacted in an aqueous solution [33].

The deconvolution of the spectra for the low C/S ratio C–S–H systems ( $C/S = 0.8$ ) suggests that in addition to the relatively small  $Q^1$  peak at  $-79.8$  ppm three other peaks exist having more negative chemical shift values. Contrary to the C–S–H ( $C/S = 1.2$ ), two peaks at about  $-83.4$  and  $-85.6$  ppm are identified for the  $C/S = 0.8$  C–S–H samples in the region for  $Q^2$  sites (Fig. 5). Both of these peaks are attributed to the  $Q^2$  sites at different silicate structural locations [36]. Their combined integral intensities were thus considered in calculating the extent of silicate polymerization. As shown in Table 1, the  $Q^2/Q^1$  ratio increases from 10.1 in the control C–S–H ( $C/S = 0.8$ ) to 24.7 and 28.1 in the C–S–H/aniline and polyaniline preparations, respectively. The peak at  $-95.4$  ppm is assigned to the  $Q^3$  site. This peak that does not exist in the high C/S ratio systems ( $C/S = 1.2$ ) is because of the cross-linking of some of the silicate tetrahedra between the C–S–H sheets [37]. The integral intensity of  $Q^3$  is increased while it is broadened when the C–S–H is organically modified. Simultaneously, the integral intensity of  $Q^2$  is decreased. It is interesting to note that an additional very broad peak in the chemical shift range of  $-100$  to  $-120$  ppm is formed in aniline and polyaniline preparations having  $C/S = 0.8$ . The existence of a peak in this area that represents  $Q^4$  sites [38] has not been reported previously for polymer-modified C–S–H systems. This is indicative of a significant increase in the silicate polymerization of the C–S–H structure. The formation of  $Q^4$  sites may also imply that the structural integrity and mechanical performance of the polymer-modified C–S–H nanocomposites would be increased.

#### Fourier transform infrared spectroscopy (FTIR)

The FTIR spectra of the phase pure and organically modified C–S–H systems are shown in Fig. 6. The characteristic set of bands in the range of  $750$ – $1,250$   $\text{cm}^{-1}$  in all

samples is due to stretching vibrations of Si–O bonds in the C–S–H [39–41]. The location of the main high intensity band in this region is indicated in Table 2 for various C–S–H materials. This band is associated with the  $Q^2$  silicon sites [40, 41]. The average values of the frequency for this vibration are about 967 and 957 cm<sup>-1</sup> for the C–S–H systems having a C/S = 0.8 and 1.2, respectively. The somewhat higher vibration frequency of this band for lower C/S ratio material is an indication of higher level of silicate polymerization in the C–S–H [40]. It is also observed that the location of this band is slightly shifted toward higher frequencies when the C–S–H is interacted with aniline and during the subsequent formation of polyaniline, again suggesting the increase in the polymerization of the silicate structure in organically modified C–S–H systems. In addition, the intensity of the bands at higher frequencies on the left shoulder of the main  $Q^2$  band increases. It is also noted that a high frequency band appears at about 1,210 cm<sup>-1</sup> in the C–S–H/polyaniline sample (C/S = 0.8, Fig. 6c). This band is most likely due to the existence of  $Q^3$  silicate sites [41]. These results are consistent with the observations from the <sup>29</sup>Si MAS NMR (discussed in the previous section) indicating that the interaction of C–S–H with organic molecules increases the polymerization extent of the silicate tetrahedra. Samples having C/S = 1.2 contain double bands at 790 and 815 cm<sup>-1</sup> that are assigned to the Si–O stretching of the  $Q^1$  tetrahedra. These bands are not present for C/S = 0.8 materials.

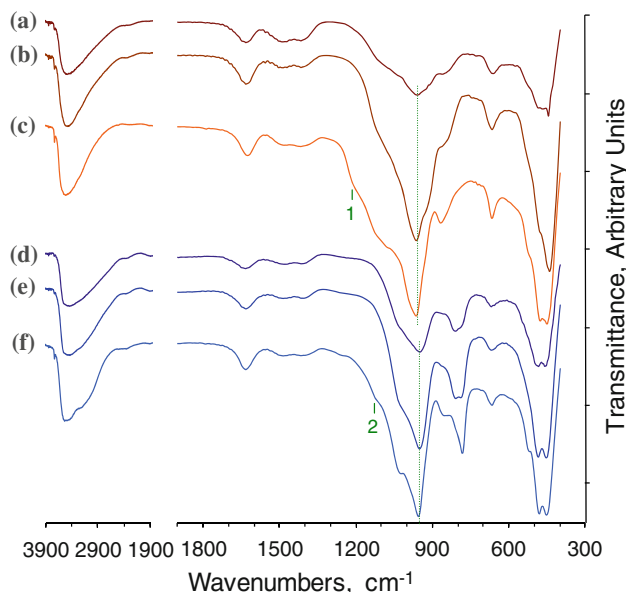


**Fig. 6** The FTIR spectra of (a) C–S–H (C/S = 0.8), (b) C–S–H/aniline (C/S = 0.8), (c) C–S–H/polyaniline (C/S = 0.8), (d) C–S–H (C/S = 1.2), (e) C–S–H/aniline (C/S = 1.2), (f) C–S–H/polyaniline (C/S = 1.2). The location of the main band in C–S–H is identified by the dotted line. Bands marked as 1 and 2 are associated with the Si–O (in  $Q^3$  and possibly  $Q^4$  sites) and polyaniline, respectively

**Table 2** The frequency (cm<sup>-1</sup>) of the main FTIR band for the C–S–H

	C/S = 0.8	C/S = 1.2
C–S–H	964	957
C–S–H/aniline	968	957
C–S–H/polyaniline	968	960

The FTIR spectrum of pure polyaniline (not shown) contains a main band at about 1,110 cm<sup>-1</sup> due to the vibration of C–N groups [17, 42]. This band appears on the shoulder of the primary band of the C–S–H/polyaniline sample (C/S = 1.2, Fig. 6f) which is easily identified when compared with the spectra of the C–S–H and C–S–H/aniline (Fig. 6d, e). For C/S = 0.8 preparations, this band overlaps with the band in the phase pure C–S–H sample. However, it appears that its relative intensity increases in the polymerized systems. This may be indicative of an interaction between polyaniline and the surface of C–S–H. The presence of other polyaniline bands in the C–S–H–polymer materials can not be distinguished due to their low intensity and overlap with the bands from C–S–H. Nevertheless, the absorption bands at about 2,300–2,800 cm<sup>-1</sup> and 3,200–3,400 cm<sup>-1</sup>, could be attributed to the interaction of NH and NH<sup>+</sup> groups present in polyaniline chains on the C–S–H surface [43].

The set of bands in the region 400–750 cm<sup>-1</sup> is characteristic of Si–O–Si deformation. These bands are well-defined in the C/S = 1.2 samples. The stretching bands due to water are located at 1,650 and 3,550 cm<sup>-1</sup> [39]. The Ca–OH vibration results in the formation of a band at 3,750 cm<sup>-1</sup>. This band becomes sharper in the organically modified C–S–H samples. The remaining bands at about 870, 1,430, and 1,500 cm<sup>-1</sup> are associated with the carbonates [41].

## Concluding remarks

C–S–H based polymer modified nanostructures were prepared by in situ polymerization method. Two different C–S–H systems (C/S = 0.8 and 1.2) were investigated. C–S–H was produced in the presence of aniline monomers that were subsequently polymerized by an oxidant. There are several indications, obtained using a variety of analytical methods, which suggest the organic phases are intimately interacted with the nanostructure of C–S–H. It is observed that the C–S–H/polyaniline samples have a higher level of silicate polymerization, the extent of which depends on the stoichiometry of the C–S–H. It is therefore possible to engineer various types of cement-based nanocomposite systems by varying the chemical composition of

the inorganic host. The interaction of polyaniline with the C–S–H may be improved through various methods such as conducting the reactions at temperatures higher than ambient, increasing the concentration of the monomer in the solution or increasing the hydration and polymerization times. The experimental characterizations presented in this study provide indirect evidence for further potential enhancement of the mechanical performance and durability of the C–S–H/polymer nanohybrids. A more detailed investigation in this regard is the subject of a separate study.

## References

- Pellenq RJ-M, Lequeux N, Van Damme H (2008) *Cem Concr Res* 38:159
- Beaudoin JJ, Patarachao B, Raki L, Alizadeh R (2009) *J Am Ceram Soc* 92(1):204
- Beaudoin JJ, Drame H, Raki L, Alizadeh R (2008) *J Mater Res* 23(10):2804
- Beaudoin JJ, Drame H, Raki L, Alizadeh R (2009) *Mater Struct* 42(7):1003
- Matsuyama H, Young JF (1999) *Chem Mater* 11:16
- Matsuyama H, Young JF (1999) *J Mater Res* 14:3379
- Matsuyama H, Young JF (1999) *J Mater Res* 14:3389
- Mojumdar SC, Raki L (2005) *J Therm Anal Calorim* 82:89
- Mojumdar SC, Raki L (2006) *J Therm Anal Calorim* 85:99
- Minet J, Abramson S, Bresson B, Franceschini A, Van Damme H, Lequeux N (2006) *J Mater Chem* 16:1379
- Franceschini A, Abramson S, Mancini V, Bresson B, Chassenieux C, Lequeux N (2007) *J Mater Chem* 17(9):913
- Minet J, Abramson S, Bresson B, Sanchez C, Montouillout V, Lequeux N (2004) *Chem Mater* 16:3955
- Alexandre M, Dubois P (2000) *Mater Sci Eng* 28:1
- Grim RE (1962) *Applied clay mineralogy*. McGraw-Hill, New York, p 422
- Alizadeh R (2009) PhD thesis, Department of Civil Engineering, University of Ottawa, p 231
- Zeng QH, Wang DZ, Yu AB, Lu GQ (2002) *Nanotechnology* 13:549
- do Nascimento GM, Constantino VRL, Landers R, Temperini MLA (2004) *Macromolecules* 37:9373
- Wu Q, Xue Z, Qi Z, Wang F (2000) *Polymer* 41:2029
- Wu C-S, Huang Y-J, Hsieh T-H, Huang P-T, Hsieh B-Z, Han Y-K, Ho K-S (2008) *J Polym Sci* 46:1800
- Alizadeh R, Beaudoin JJ, Ramachandran VS, Raki L (2009) *J Adv Cem Res* 21(2):59
- Dramé H, Beaudoin JJ, Raki L (2007) *J Mater Sci* 42:6837. [10.1007/s10853-006-1328-5](https://doi.org/10.1007/s10853-006-1328-5)
- Alizadeh R, Beaudoin JJ, Raki L (2010) *Mater Struct*. doi:[10.1617/s11527-010-9605-9](https://doi.org/10.1617/s11527-010-9605-9)
- Makar J, Chan GW (2008) *J Am Ceram Soc* 91(4):1292
- Popova A, Geoffroy G, Renou-Gonnord M-F, Faucon P, Gartner E (2000) *J Am Ceram Soc* 83(10):2556
- Merlin F, Lombois H, Joly S, Lequeux N, Halary J-L, Van Damme H (2002) *J Mater Chem* 12:3308
- Feldman RF, Ramachandran VS (1974) *Cem Concr Res* 4(2):155
- Choi HJ, Lee JH, Cho MS, Jhon MS (1999) *Polym Eng Sci* 39(3):493
- Yang C, Fang Z, Liu J, Liu W, Zhou H (2000) *Thermochim Acta* 352–353:159
- Binitha NN, Sugunam S (2008) *J Appl Polym Sci* 107:3367
- Liu C, Zhou Y, Li S, Li L, Yu M (2008) *Polym Adv Technol* 19(12):1693
- Kalousek GL (1954) *Proceedings of the third international symposium on the chemistry of cement*, London, UK, p 296
- Ramachandran VS, Beaudoin JJ (eds) (2001) *Handbook of analytical techniques in concrete science and technology*. William Andrew, NY, p 964
- Beaudoin JJ, Raki L, Alizadeh R (2009) *Cem Concr Compos* 31(8):585
- Massiot D, Fayon F, Capron M, King I, Le Calvé S, Alonso B, Durand J-O, Bujoli B, Gan Z, Hoatson G (2002) *Magn Reson Chem* 40(1):70
- Chen JJ, Thomas JJ, Taylor HFW, Jennings HM (2004) *Cem Concr Res* 34(9):1499
- Klur I, Pollet B, Virlet J, Nonat A (1998) *2nd international conference on NMR spectroscopy of cement based materials*, p 119
- Cong X, Kirkpatrick RJ (1996) *Adv Cem Based Mater* 3:144
- Wieker W, Grimmer A-R, Winkler A, Mägi M, Tarmak M, Lippmaa E (1982) *Cem Concr Res* 12:333
- Delgado AH, Paroli RM, Beaudoin JJ (1996) *Appl Spectrosc* 50(8):970
- Yu P, Kirkpatrick RJ, Poe B, McMillan PF, Cong X (1999) *J Am Ceram Soc* 82(3):742
- Loderio IG, Macphee DE, Palomo A, Fernandez-Jimenez A (2009) *Cem Concr Res* 39:147
- Lee D, Char K, Lee SW, Park YW (2003) *J Mater Chem* 13:2942
- Sudha JD, Sasikala TS (2007) *Polymer* 48:338